

# Radiative Recombination Plasma Rate Coefficients for Multiply Charged Ions

Stephan Fritzsche <sup>1,2,3,\*</sup> , Anna V. Maiorova <sup>1,2</sup>  and Zhongwen Wu <sup>1,4</sup> <sup>1</sup> Helmholtz-Institut Jena, Fröbelstieg 3, 07743 Jena, Germany<sup>2</sup> GSI Helmholtzzentrum für Schwerionenforschung, 64291 Darmstadt, Germany<sup>3</sup> Theoretisch-Physikalisches Institut, Friedrich-Schiller-Universität Jena, 07743 Jena, Germany<sup>4</sup> Key Laboratory of Atomic and Molecular Physics & Functional Materials of Gansu Province, College of Physics and Electronic Engineering, Northwest Normal University, Lanzhou 730070, China

\* Correspondence: s.fritzsche@gsi.de

**Abstract:** Radiative recombination (RR) plasma rate coefficients are often applied to estimate electron densities and temperatures under quite different plasma conditions. Despite their frequent use, however, these rate coefficients are available only for selected (few-electron) ions and isoelectronic sequences, mainly because of the computational efforts required. To overcome this limitation, we report here a (relativistic) cascade model which helps compute fine-structure and shell-resolved as well as total RR plasma rate coefficients for many, if not most, elements of the periodic table. This model is based on JAC, the Jena Atomic Calculator, and supports studies on how the electron is captured in selected levels of the recombined ion, a relativistic (Maxwellian) electron distribution, or how the multipoles beyond the electric-dipole field in the electron-photon interaction affect the RR rate coefficients and, hence, the ionization and recombination dynamics of hot plasma. As a demonstration of this model, we compute, compare, and discuss different RR plasma rate coefficients for initially helium-like ions, with an emphasis especially on Fe<sup>24+</sup> ions.

**Keywords:** astrophysics; atomic cascade; atomic structure; dielectronic recombination; level and excitation energies; Jena Atomic Calculator; plasma rate coefficient; radiative recombination; relativistic; transition amplitude



**Citation:** Fritzsche, S.; Maiorova, A.V.; Wu, Z. Radiative Recombination Plasma Rate Coefficients for Multiply Charged Ions. *Atoms* **2023**, *11*, 50. <https://doi.org/10.3390/atoms11030050>

Academic Editors: Sultana N. Nahar and Anand K. Bhatia

Received: 23 December 2022

Revised: 22 January 2023

Accepted: 1 March 2023

Published: 4 March 2023



**Copyright:** © 2023 by the authors. Licensee MDPI, Basel, Switzerland. This article is an open access article distributed under the terms and conditions of the Creative Commons Attribution (CC BY) license (<https://creativecommons.org/licenses/by/4.0/>).

## 1. Introduction

The radiative recombination (RR) of an ion refers to the capture of a free electron under the emission of one or several photons [1–4]. Often, photons with a rather wide range of frequencies contribute to this recombination process, even for free electrons of given energy, since they can first be captured into any excited state of the ion, and before the ion further stabilizes by characteristic photon emission. While the most prominent photon spectra in astrophysics usually arise from either hydrogen or helium, owing to their high cosmic abundances, direct recombination lines and peak structures have also been observed in several other elements, including medium and heavy ones [5,6]. From these spectra, moreover, the plasma temperature and density can be derived by means of RR plasma-averaged rate coefficients and, hence, information on the temporal evolution of different plasma environments [7,8]. Therefore, fast and reliable predictions of the RR cross sections and plasma rate coefficients are frequently needed for those recombination lines, which are neither blended by stronger lines nor contaminated due to other de-excitation mechanisms.

Various tabulations exist today for RR plasma rate coefficients among different isoelectronic sequences [9–14]. These (and several further) compilations either list the rate coefficients explicitly, or provide fit formulas in order to express their temperature dependence over a wide range of, say,  $10^3 \dots 10^8$  K, and in selected cases even up to relativistic temperatures  $\lesssim 10^{10}$  K. Despite their repeated use, however, many of the available RR

plasma rate coefficients are built until the present upon photoionization cross sections of the ground and, perhaps, a few low-lying levels alone as well as the electric-dipole (E1) approximation. Further limitations in employing such rate coefficients arise from inaccurate computations, the use of restricted ionization data (when simply based on the Milne relation) or some ill-suited electron distribution in the convolution over the free plasma electrons [15–17]. While good progress in designing collisional-radiative models and codes has been made for plasma spectroscopy [18], these limitations still make uninvolved access to and dedicated tools for the computation of RR plasma rate coefficients highly desirable.

Whereas most RR plasma rate coefficients exhibit a rather smooth behavior, if drawn as function of the plasma temperature, detailed ab initio calculations are usually required for understanding the role of (i) the charge state of ions, (ii) their initial level population, (iii) the capture into high-lying shells, or how (iv) non-E1 contributions in the electron-photon interaction affect the RR process. In addition, (v) relativistic and local modifications of the electron distribution in the plasma might influence the recombination dynamics. Until the present, however, rather little is known about all these dependencies. Finally, (vi) microphysical processes may also modify the observed astrophysical spectra since their plasma is often diluted and far from any thermodynamic equilibrium [19,20].

In this work, we report a (relativistic) cascade model that helps compute fine-structure level- and shell-resolved as well as total RR plasma rate coefficients for many, if not most, elements of the periodic table. This model is based on JAC, the Jena Atomic Calculator [21], and it enables one to explore not only the dependencies (i–iv), which arise from the electronic structure of the ions and their interaction with the radiation field, but also the modifications (v–vi) owing to the plasma itself. In this cascade model, all (electron) configurations and continua relevant for the given plasma conditions are determined and incorporated—more or less—automatically into the computations. As a demonstration of the implemented model, we shall compute, compare, and discuss different RR plasma rate coefficients of initially helium-like ions, with an emphasis especially upon Fe<sup>24+</sup> ions. Since these tools enable one to calculate RR plasma rate coefficients also for ions with rather complex shell structure, the present expansion of the JAC toolbox may also facilitate surveys of the RR process along different isoelectronic sequences.

This work is organized as follows. In Section 2, we first recall the basic formulas and notations for characterizing the RR process in terms of cross sections and rate coefficients. This also includes a brief account on the RR cascade scheme, suitable for different (open-shell) structures, and how this scheme is implemented into the JAC toolbox. Results are shown in Section 3 for the RR into initially helium-like ions and are compared with data from the literature as well as semi-empirical estimates. This comparison shows the influence of high-lying shells in the capture of free electrons. It also manifests how the multipole fields beyond E1 contribute to the ionization and recombination dynamics of plasma with highly charged ions.

## 2. Theory Furthermore, Computations

### 2.1. Radiative Recombination Cross Sections

Like the electron emission in the time-reversed atomic photoionization, the (electron) capture is usually divided into two processes: (i) the RR with its *direct* photon emission and slowly varying cross sections as functions of the electron energy as well as (ii) the dielectronic recombination (DR). The DR process arises from the excitation of re-autoionizing resonances and typically refers to rather sharp resonances in the capture cross sections [22,23]. We here restrict ourselves to the direct photon emission and the (reduced) RR transition amplitudes for levels with well-defined total symmetry

$$\left\langle \alpha_f \mathbb{J}_f \left\| \mathbb{O}^{(M,RR)} \right\| \left( \alpha_i \mathbb{J}_i, \varepsilon \kappa \right) \mathbb{J} \right\rangle = \left\langle \left( \alpha_i \mathbb{J}_i, \varepsilon \kappa \right) \mathbb{J} \left\| \mathbb{O}^{(M,\text{photoionization})} \right\| \alpha_f \mathbb{J}_f \right\rangle^*, \quad (1)$$

which are complex-conjugate to the photoionization process. These (many-electron) matrix elements therefore describe the capture of a free electron with kinetic energy  $\varepsilon$  and

angular momentum quantum number  $\kappa$  by an ion in the initial [ $N$ -electron] level  $\alpha_i \mathbb{J}_i$  with total energy  $E_i$ , and which leads—under the emission of a photon with multipolarity  $\mathbb{M} \equiv (L, p)$ —to some [ $(N + 1)$ -electron] final level of the ion below of its ionization threshold. In this notation, moreover,  $\mathbb{O}^{(\mathbb{M}, \text{RR})}$  refers to the electron-photon interaction (operator) as associated with the multipole field  $\mathbb{M}$  and  $\mathbb{J} \equiv J^P$  to both the total angular momentum and parity of each level, whereas  $\alpha_{i,f}$  stands for all further quantum numbers as required for unique specification of the corresponding fine-structure separation [24,25]. The initial and final state functions of the ion are generated self-consistently by applying, for instance, the multiconfiguration Dirac–Hartree–Fock (MCDHF) method [26,27].

While we shall not describe the MCDHF method here in further detail, we just note that it typically helps incorporate all major contributions into the electronic structure calculations. When compared with other techniques from (relativistic) many-body perturbation theory or coupled-cluster theory [28], such multiconfigurational or configuration-interaction (CI) expansions are indeed much simpler to deal with, especially if electrons occur in one or several *open* shells [29,30] or within the continuum [31]. To add a continuum electron to a given set of (non-relativistic) initial-state configurations, all  $(N + 1)$ -electron configurations state functions (CSF) are formed from the bound state which gives rise to a (well-defined) symmetry  $\mathbb{J}_t$  of the overall system. Whereas the mixing of CSF in the scattering state therefore still refers to the bound ion alone, this construction of the many-electron continuum has been found feasible and very useful for computation of all (auto-) ionization processes and atomic cascades.

In contrast to the DR, a nonzero RR amplitude (1) occurs for all kinetic energies  $\varepsilon$  of the free electron but decreases rapidly for the capture of sufficiently fast electrons. Obviously, moreover, different excitement levels  $\alpha_f \mathbb{J}_f$  of the final ion lead to different photon energies, while a good number of (initial many-electron) continua with symmetry  $(\alpha_i \mathbb{J}_i, \varepsilon \kappa) \mathbb{J}$  and multipoles  $\mathbb{M}$  may contribute to the RR cross section of each final level.

$$\sigma^{(\text{RR})}(\varepsilon; \alpha_i \mathbb{J}_i \rightarrow \alpha_f \mathbb{J}_f) = \frac{8 \alpha^3 \pi^3 \omega}{(2J_f + 1) \beta^2 \gamma^2} \sum_{\mathbb{M} \mathbb{J} \kappa} \left| \left\langle \alpha_f \mathbb{J}_f \left\| \mathbb{O}^{(\mathbb{M}, \text{RR})} \right\| (\alpha_i \mathbb{J}_i, \varepsilon \kappa) \mathbb{J} \right\rangle \right|^2, \quad (2)$$

with  $\beta = v/c$ ,  $\gamma = \sqrt{1 - \beta^2}$ , and the asymptotic velocity  $v$  of the incident electron. Indeed, these (final) level-resolved RR cross sections can be readily calculated within the JAC toolbox and need not to be further elaborated here.

### 2.2. Temperature-Dependent Plasma Rate Coefficients

RR plasma rate coefficients generally describe the effective recombination rate of an ion in a plasma with unit electron density. Because of the level dependence of the RR cross sections (2), different RR plasma rate coefficients can be readily distinguished owing to the number of final ionic levels  $\alpha_f \mathbb{J}_f$  that are taken into account in the summation. Moreover, the total RR plasma rate coefficient is obtained from the convolution of the (total) RR cross section for an ion, initially in the level  $\alpha_i \mathbb{J}_i$ , with an isotropic Maxwellian distribution function of the free electrons in a plasma with temperature  $T_e$

$$\alpha^{(\text{RR})}(T_e; i) = \frac{4}{(k_B T_e)^{3/2} \sqrt{2\pi} m} \int_0^\infty d\varepsilon \varepsilon \left[ \sum_{\alpha_f \mathbb{J}_f} \sigma^{(\text{RR})}(\varepsilon; \alpha_i \mathbb{J}_i \rightarrow \alpha_f \mathbb{J}_f) \right] \exp\left(-\frac{\varepsilon}{k_B T_e}\right) \quad (3)$$

and electron mass  $m$ , and often given in units  $\text{cm}^3/\text{s}$ . In this expression, the summation over  $\alpha_f \mathbb{J}_f$  formally runs over all bound levels of the final ion, including its Rydberg levels and, perhaps, further valence-shell excitations. In practice, however, this summation is usually truncated to the relevant low-lying levels as well as to just a few selected electron continua, owing to the well-established selection rules for the electron-photon interaction. If, for instance, we restrict this summation to a single fine-structure level  $\alpha_f \mathbb{J}_f$  or a single shell  $n\ell$ , i.e., with  $\{\alpha_f \mathbb{J}_f \equiv (\alpha_i \mathbb{J}_i, n\ell) \alpha_f \mathbb{J}_f\}$  in the summation above,

the same expression (3) gives rise to either fine-structure resolved plasma rate coefficient  $\alpha^{(RR)}(T_e; i \rightarrow f)$  or to shell-resolved rate coefficient  $\alpha^{(RR)}(T_e; i \rightarrow (i, n\ell))$ , respectively. These *restricted* RR rate coefficients frequently occur in the literature, in particular if the RR cross sections are based on photoionization data and if use is made of the (so-called) Milne relation [32], since detailed photoionization cross sections of initially excited levels are hardly accessible. Although the distinction of these fine-structure and shell-resolved as well as the total RR plasma rate coefficient appears to be quite simple, their difference is seldom mentioned at all in the literature, and this may cause serious confusion for the readers, especially when RR rate coefficients from different sources need to be compared to each other. Since, moreover, the rate coefficients arise from a convolution of the cross section with a (Maxwellian) distribution of the free electrons in a plasma, these rate coefficients are explicitly temperature-dependent and are just defined in the low-density limit of the plasma, though they remain useful also for most astrophysical and technical plasma. For more realistic plasma environments, a depression of the ionization threshold typically occurs and may result not only into a ‘cut-off’ of excited levels, into which electrons are captured, but also into some lowering of the associated plasma rate coefficients.

Most computations of plasma rate coefficients in the literature simply apply RR cross sections that are based on the (E1) dipole approximation, a Maxwellian distribution of electrons as well as a more or less well-chosen truncation of the final levels in expression (3). The truncation of the (number of) valence shells  $n\ell$  is hereby closely related to the electronic structure of the ions of interest and the rapidly decreasing cross sections for the capture into high- $n$  shells. From our notation of the RR transition amplitude (1), however, it is easily seen how the contributions of the higher multipoles M1, E2, etc. of the radiation field can be taken into account and either result in additional terms to the existing E1 amplitudes, or even open new RR capture channels beyond the electric-dipole (E1) approximation. Since each of the multipole transition amplitudes obeys its own scaling with regard to the nuclear charge  $Z$  of the ions, they will be relevant for different elements, shell structures, and energies of the free electrons. Below, we will show how these multipole contributions can be willingly controlled in our cascade implementation.

For high-enough temperatures, the electrons in the plasma *do* no longer follow the (non-relativistic) Maxwellian distribution as assumed in the rate coefficients above. At these temperatures, a relativistic Maxwellian distribution  $f(E) dE$ , normalized to unity, is given by [6]

$$f(E)dE = \frac{\sqrt{E(E^2 - 1)}}{\Theta e^{1/\Theta} K_2(1/\Theta)} \exp\left(-\frac{E - 1}{\Theta}\right) dE, \quad \Theta(T_e) = \frac{k_B T_e}{m c^2},$$

where  $E$  is the total energy of the plasma electrons, in units of  $m c^2$ , and  $\Theta(T_e)$  the dimensionless temperature normalized as well to the rest mass of the electron. Moreover,  $K_2(x)$  denotes the modified Bessel function of second order. The influence of such a relativistic distribution function upon the RR plasma rate coefficients was first pointed out (and explicitly treated) by Trzhaskovskaya and coworkers [33]. This relativistic Maxwellian distribution of the plasma electrons can be accounted for in the RR plasma rate coefficients by a temperature-dependent factor

$$\alpha^{(RR:relativistic)}(T_e; i \dots) = F^{(relativistic)}(\Theta) \alpha^{(RR)}(T_e; i \dots)$$

$$F^{(relativistic)}(\Theta) = \frac{\sqrt{\frac{\pi}{2}} \Theta}{e^{1/\Theta} K_2(1/\Theta)} \approx \frac{1}{\left(1 + \frac{15}{8} \Theta + \frac{105}{128} \Theta^2 + \dots\right)} \quad \text{for } \Theta \lesssim 1.$$

This factor  $F^{(relativistic)}(\Theta)$  becomes relevant in the computation of RR plasma rate coefficients for electron temperatures  $T_e \gtrsim 10^8$  K and can be readily incorporated into the cascade simulations below.

### 2.3. Radiative Recombination Cascades

As for many other atomic processes, the calculation of RR cross sections and plasma rate coefficients can always be traced back to the many-electron amplitudes (1) and, hence, to a reasonably accurate representation of all the initial and final levels, which are involved into the capture process. In practice, both the representation as well as the number of these atomic bound states and (free-electron) continuum orbitals require special care and often make the major difference among the available implementations. Because of the—formally infinite—number of final states of the recombined ions, moreover, correlations are usually treated in rather an ad hoc manner. Therefore, in order to support realistic and systematically enlarged studies on plasma rate coefficients, a good and simple control is needed for the number of final states to be included, the multipoles of the interacting photon field, the choice and discretization of the free-electron (waves), the set-up of atomic potentials, as well as for the associated configuration mixing, to just mention the main influences. All these choices do eventually affect the plasma rate coefficients, although little is known to which precise extent.

We here wish to formalize (and simplify) the calculation of RR plasma rate coefficients by applying a radiative-recombination cascade (model). While such a cascade model naturally includes fewer correlations in representing the relevant atomic levels, it supports a much greater flexibility in modeling the capture into high- $n$  shells or for the treatment of the electron continua. For such a cascade of competing RR processes, the rate coefficients are obtained from the computation and the subsequent simulation of an associated RR cascade scheme. Several rather analogous schemes have been implemented before in the JAC toolbox [34] for dealing, for instance, with the DR plasma rate coefficients [23], the stepwise decay of inner-shell hole states [35–37], the photoexcitation with subsequent decay [38], or the decay of hollow ions [39]. In contrast to the decay of (inner-shell) excited atoms and ions, the radiative and dielectronic cascades (schemes) refer in JAC not to a series of subsequent but rather competing capture processes. Despite this different interpretation, however, the concept of a cascade facilitates the implementation and has suggested treating the (RR) plasma rate coefficients here in quite an analog form.

For the recently implemented RR cascades scheme, the computation starts from the representation of the initial level  $\alpha_i \mathbb{J}_i$  and a set of automatically generated configurations, which can be formed due to the capture of one additional electron. Obviously, such a cascade scheme is in contrast to the computation of “well-correlated” capture amplitudes (1), as perhaps an appealing alternative, but which typically comes at a formidable price: apart from the sheer size of all required many-electron wave functions and scattering states, the understanding and interpretation of individual terms are quickly lost in a correlated approach as the representation of the scattering and final states will then necessarily be distributed among (many) different configurations.

An efficient computation of RR plasma rate coefficients requires, of course, a simple control (and handling) of the radiative amplitudes for all electrons, which contributes substantially due to their energy  $\varepsilon$  and to the integral on the right-hand side of Equation (3). Apart from a suitable discretization of the kinetic energies  $\varepsilon$ , the number of photorecombination channels in particular often grows rapidly, if an additional electron is coupled to the initial ionic core configuration. In the cascade implementation below, we therefore restrict ourselves to placing the captured electron into the valence or any higher shell but for just a given range of  $n$  and  $\ell$  values. A choice of  $n \lesssim 20$  and  $\ell \lesssim 4$  has been found sufficient for most ions [40], although further tests are needed (and suggested) in order to monitor the stability and convergence of the rate coefficients. The contributions of the shells with higher principal quantum number  $n$  could be estimated also using, for instance, the semi-empirical formulas by Kramers [41] or Kotelnikov and Milstein [42], and for which additional procedures are provided by the JAC toolbox. For the computation of the RR rate coefficients, moreover, a temperature-dependent Maxwellian distribution is usually assumed for the free electrons, which can be truncated to, say, 5–10 times the mean

free-electron energy in the plasma, in line with the characteristic lowering  $\sim (I_p + \varepsilon)^{-7/2}$  of the RR cross sections as the free-electron energy  $\varepsilon$  increases.

#### 2.4. Implementation of Plasma Rate Coefficients into the JAC Toolbox

Atomic cascades have been the focus of developing the JAC toolbox during recent years [43,44]. Such cascades are ubiquitous in nature and need to be analyzed in rather different contexts, from precision measurements to the modeling of astrophysical spectra, and up to the radiation damage in biological matter. In the past, however, almost any quantitative analysis has failed because of the inherent complexity of such cascades. For the RR of ions in plasma, for example, one needs to access and combine a large number of the photorecombination amplitudes (1) in order to model the capture of free electrons at all final levels  $\alpha_f \mathbb{J}_f$  of interest. In contrast to this “number problem”, the plain use and manipulation of these continuum states have been found helpful also for implementing approximate atomic Green functions [45] as well as various second-order processes in the interaction with the radiation field [25].

The modeling of most atomic cascades suggests clearly distinguishing between (so-called) cascade computations and cascade simulations [34]. Whereas the cascade computations aim to generate all the (computationally) expensive amplitudes, the subsequent simulations then serve to combine these data and to extract the desired information, e.g., the plasma rate coefficients in the present case. For the computation of an RR cascade (scheme), for instance, one starts from the capture of an electron in any of the pre-specified  $n\ell$  shells, which needs to be coupled properly to the initial level  $\alpha_i \mathbb{J}_i$  of the ion. Typically, the prior cascade computations cause the major computational effort as they require a (more or less) self-consistent representation of all the atomic levels involved in the recombination process. These cascade computations should be performed independently of both the temperature or the (summation of) final levels  $\sum_{\alpha_f \mathbb{J}_f} \dots$ , for which the plasma rate coefficients need to be derived eventually, once a suitable list of such transition amplitudes is available. The subsequent cascade simulations are much faster than the prior computations and they can often be based even on the same set of amplitudes.

All (cascade) computations in this work are built on the JAC toolbox, which is suitable for most atoms and ions from the periodic table, in order to compute level energies, energy shifts, rates, and cross sections for different atomic processes and experimental setups [21,24]. Figure 1 displays a few selected features of this toolbox, though with special emphasis on the radiative recombination of multiply charged ions and the calculation of plasma rate coefficients. Apart from the relativistic description of the electronic structure and properties of free atoms and ions, as appropriate for medium and heavy elements, we aim with this toolbox to integrate different atomic processes within a single computational framework and, hence, to ensure good self-consistency of the generated data. JAC itself is implemented in Julia, a new programming language for scientific computing, which is known to include a good number of (modern) features, such as dynamic types, optional type annotations, just-in-time compilation of code, dynamic code loading or garbage collection [46,47]. As typical for the JAC toolbox, correlated RR cross sections can be calculated as well by means of an `Atomic.Computation`, if the proper settings are provided by the user for the `PhotoRecombination` module. These computations are organized analog to calculating most other atomic processes within JAC, and where all the requested (photorecombination) amplitudes are always obtained from the associated module. The implementation of a radiative-recombination cascade scheme, in contrast, includes fewer correlations in the representation of the atomic levels but supports a much greater flexibility in dealing with the capture into high- $n$  shells, the discretization of the electron continuum or the desired temperature range of the plasma.

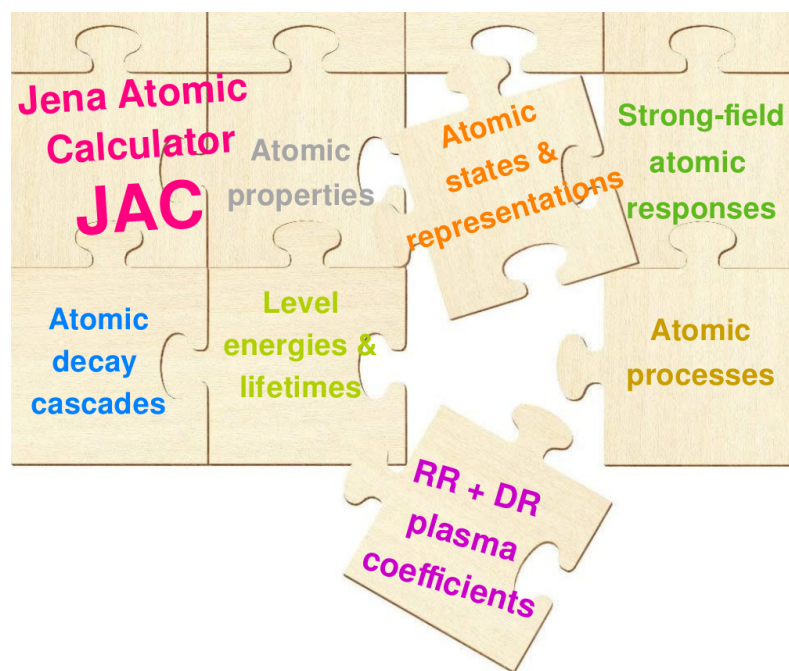


**Figure 1.** Selected features of the JAC toolbox [21] that help compute the level structure, processes and cascades of most atoms and ions across the periodic table. Here, emphasis has been placed on the radiative recombination of multiply charged ions and several associated plasma rate coefficients. Apart from the recombination of ions, this toolbox supports several further (relativistic) computations as briefly brought up in this jigsaw puzzle.

### 2.5. Data Types for Radiative Recombination Cascades

To facilitate the communication *with* and the data transfer *within* the program, the JAC toolbox is built on a rather sizable hierarchy of data structures. These structures aim to identify useful and frequently recurring objects in the representation and treatment of atomic behaviors and processes. They also form the language elements in order to readily describe and control the desired computations. Two prominent examples for such data structures are an `Orbital` for specifying the quantum numbers and radial components of single-electron orbital functions, or a `Level` for the full representation of a single level  $\alpha \mathbb{J}$ , which then encompasses all information about the radial wave functions, the coupling of the angular momenta as well as the mixing (and number) of configuration state functions within the given basis. In total, there are at present about  $\sim 250$  of these data structures in JAC, though most of them remain hidden to the user of the toolbox. As usual, this set of data structures needs to be enlarged by a few items if the code is expanded toward new features. While we shall not discuss details of the current implementation, we here explain the data (structure) that has been designed in order to deal with general RR cascade schemes.

Figure 2 displays the definition of the data structure `Cascade.Radiative RecombinationScheme` in JAC, which helps perform all the RR cascade computations below. Apart from the multipoles of the radiation field, which are to be included into the photorecombination process, this cascade scheme enables one to select the partial waves of the free electron, e.g., the orbital angular momentum values (`lValues`) as well as the maximum and number of the free-electron energies in the discretization of the electron continuum. Whereas the integration  $\int_0^\infty d\varepsilon \dots$  in the rate coefficient (3) runs formally over all positive kinetic energies  $\varepsilon > 0$ , we internally make use of a Gauss–Legendre integration in order to keep the energy discretization simple and independent of the temperature  $T_e$ , for which plasma rate coefficients are to be evaluated in subsequent simulations. Often a maximum energy  $\varepsilon_{\max} \approx 5 \times k_B T_{e,\max}$  and an energy mesh of about 12–24 points have been found sufficient in order to obtain plasma rate coefficients with 15–20% accuracy. For ions with a complex (valence) shell structure, further work is, however, needed to

better understand how these rate coefficients depend on details of the energy discretization. The structure `Cascade.RadiativeRecombinationScheme` also requires the user to provide a list of nonrelativistic subshells (`intoShells`) into which the electrons are to be placed, in addition to those shells that already belong to the ionic core. The specification of the core occupation (i.e., of the initial levels  $\alpha_i \mathbb{J}_i$  of the ions) in terms of one or several reference configurations is common to all cascade schemes and is provided independently to the cascade computations. Indeed, such a flexible but powerful description of the shell occupation as well as all further input have been found relevant and necessary for covering a wide range of possible applications of RR plasma rate coefficients.

```

Cascade.RadiativeRecombinationScheme
struct Cascade.RadiativeRecombinationScheme <: Cascade.AbstractCascadeScheme
... a structure to define and describe the radiative recombination of an atom or ion
in some initial state/configuration; in this scheme, all the configurations that
follow from the capture of an additional electron are generated automatically.
These configurations are selected by the list of intoShells (nl), into which a
capture may occur. The initial electron continua are determined by means of the
partial waves (lValues), the maximum as well as the number of free-electron
energies for the (Gauss-Legendre) integration of the plasma rate coefficients.
The maximum electron energy has to be given in line with the maximum temperature
T_e,max, for which RR plasma rate coefficients are later to be extracted in the
subsequent cascade simulations; cf. Basics.convertUnits().

+ multipoles                ::Array{EmMultipole}
... Multipoles of the radiation field that are to be included into the
photorecombination.
+ lValues                   ::Array{Int64,1}
... Orbital angular momentum values of the free-electron, for which partial waves
are considered for the RR.
+ NoFreeElectronEnergies ::Int64
... Number of free-electron energies that are chosen for a Gauss-Laguerre
integration.
+ maxFreeElectronEnergy ::Float64
... Maximum free-electron energies that restrict the energy of free-electron orbitals
in the photorecombination of plasma electrons. This maximum energy has to be
derived from the maximum temperature, for which RR plasma coefficients need to
be obtained, and is typically set to about 5 x T_e,max.
+ electronEnergyShift ::Float64
... Energy shift [a.u.] for all final bound-state energies relative to the levels
from the reference configuration; this is realized by shifting the initial level
energies by the negative amount.
+ minPhotonEnergy ::Float64
... Minimum (mean) photon energy [in a.u.] for which radiative capture amplitudes
are calculated, in practice.
+ intoShells                ::Array{Shell,1}
... List of shells into which electrons are placed (captured) for the representation
of the final levels alpha_f J_f.

```

**Figure 2.** Definition of the data structure `Cascade.RadiativeRecombinationScheme` in JAC that helps perform the cascade computations in Section 3 below. It is one of the supported cascade schemes of a `Cascade.Computation` and enables the user to specify the multipole components of the radiation field in the photorecombination of the ion, the partial waves of the incoming free electrons, the discretization of the free-electron continuum, as well as the shells into which electrons are to be captured. See text for further explanations.

Apart from the RR cascade scheme above, a hierarchy of cascade *approaches* has been defined within the JAC toolbox to keep the computations overall feasible. These approaches are mainly differentiated by the quantum-mechanical representation of the level structures and, thus, enable the user to control the extent to which interelectronic correlations are to be taken into account. By default, a single-configuration approach is chosen, in which the (final) configurations of the recombined ion are built by the capture of an additional electron to a set of (bound) reference configurations as well as by a configuration-interaction expansion of the associated fine-structure levels. In this approach, configuration mixing

is restricted to a single nonrelativistic configuration at a given time. To improve the representation of the fine-structure levels, strongly interacting configurations could also be *grouped* together, although such a (user-selected) multiconfiguration approach is only partly supported at present. In the next section, we show how such cascade computations can be performed for initially helium-like  $\text{Fe}^{24+}$  ions, and along with the ensuing cascade simulations for extracting the desired rate coefficients.

### 3. Radiative Reombination Plasma Rate Coefficients for Multiply Charged Ions

While the RR plasma rate coefficients are known to decrease smoothly with (increasing) electron temperature, detailed computations are typically needed to predict their explicit dependence for (i) different charge states of the ion, (ii) its initial level population, (iii) the capture into selected and, perhaps, high-lying shells, or to explain how (iv) non-E1 contributions affect the RR in various multiplied and highly charged ions. To date, rather little is known about all these dependencies, not to mention a simple and reliable access to the RR plasma rate coefficients is not known at all [48–50], despite all the efforts in developing realistic collisional-radiative models for different plasma environments [51]. Although, for the sake of simplicity and comparison, we shall restrict all examples below to the RR into initially helium-like ions, our implementation above is also suitable for dealing with open-shell structures as they frequently occur in astrophysics and fusion research.

#### 3.1. Plasma Rate Coefficients for Initially $\text{Fe}^{24+}$ Ions

Let us start with the RR of initially helium-like iron  $\text{Fe}^{24+}$  ions owing to their abundance in different astrophysical objects. The rate coefficients for these ions have attracted recurring interest in the literature. They have been found significant for both photo- and collisionally-ionized plasma, and at various temperatures  $T \lesssim 10^8$  K [52,53]. Therefore, the RR of an initially helium-like iron  $\text{Fe}^{24+}$  ions provides a good and simple test-bed for the implementation and computations in this work.

To calculate plasma rate coefficients in the framework of JAC [21], we need first to run a cascade computation. In this computation, all the relevant final-state configurations are generated automatically, and the associated fine-structure levels are evaluated, in turn, in order to compute the RR amplitude (1). The upper panel of Figure 3 shows the input for this cascade computation into initially helium-like  $\text{Fe}^{24+}$  ions. Apart from a brief name of the computations, the specification of the grid, the nuclear charge of the ion ( $Z = 26$ ) and the initial  $1s^2$  configuration, all that has to be provided by the user is the list of partial waves of free electrons in the continuum (`lValues`) and the shells (`intoShells`), into which an electron can be captured eventually. In addition, a few parameters, specific to the radiative-recombination scheme (cf. Figure 3), help control the size of the computations. These parameters comprise the maximum energy and the number of free-electron energies in the integration of the plasma rate coefficients, a minimum photon energy for evaluating the many-electron amplitudes as well as a few others, which can be provided by the user in order to overwrite existing default values. Indeed, this input provides a rather flexible control for most open-shell ions without either the final-electron configurations nor the relevant capture amplitudes needing to be selected or specified explicitly.

Moreover, a single-configuration approach [`Cascade.SCA()`] is used by default to deal, in turn, with each final configuration of the electron capture. These configurations are built from the initial configuration(s) and an additional electron in one of the `intoShells`. In these cascade computations, the major effort refers to the calculation of the fine-structure levels for each configuration as well as to the numerical evaluation of the RR amplitudes (1). Despite its simplicity, however, the input to these computations still requires some physical insight into both the electronic structure of the initial ion and the intricacy of the associated many-electron continuum. This involvement refers, for instance, to the partial waves, the energies of the free electrons, the choice of multipoles or some prior insight, which of the excited shells are in fact relevant for the given charge state and temperatures. In these cascade computations, no attempt is internally made in order to control that all important

configurations are taken into account for the representation of the final levels  $\alpha_f \mathbb{J}_f$  (owing to the coupling of the multipoles and partial waves), nor that all the computed configurations are relevant for the rate coefficients of interest. Obviously, this insight of the user into the RR process cannot be completely formalized in advance.

```
# RR plasma rate coefficients for initially He-like ions:
# Radiative recombination cascade computation
setDefault("unit: energy", "eV")
name          = "Radiative recombination cascade for helium-like iron ions"
grid          = Radial.Grid(Radial.Grid(false), rnt = 4.0e-6, h = 5.0e-2, hp = 0.6e-2,
rbox = 10.0)
lValues       = [0, 1, 2, 3]
intoShells    = Basics.generateShellList(2, 12, "f")
excitationScheme = Cascade.RadiativeRecombinationScheme([E1], lValues, 24, 4300., 0., 0.,
intoShells)
wa           = Cascade.Computation(Cascade.Computation(); name=name,
nuclearModel=Nuclear.Model(26.), grid=grid, approach=Cascade.SCA(),
scheme=excitationScheme, initialConfigs=[Configuration("1s~2")] )
perform(wa; output=true)

# RR plasma rate coefficients for initially He-like ions:
# Radiative recombination cascade simulation
simulationSettings = Cascade.SimulationSettings(true, false, 0.)

temps = [1.0e+5, 2.15e+5, 4.63e+5, 1.0e+6, 2.15e+6, 4.63e+6, 1.0e+7] # in [K]
data = [JLD.load("Cascade-RR-rate-computations-He-like.jld")]
name = "Radiative recombination simulations for He-like ions"
prop = Cascade.RrRateCoefficients(1, temps, [E1], LevelSelection(), Configuration[])

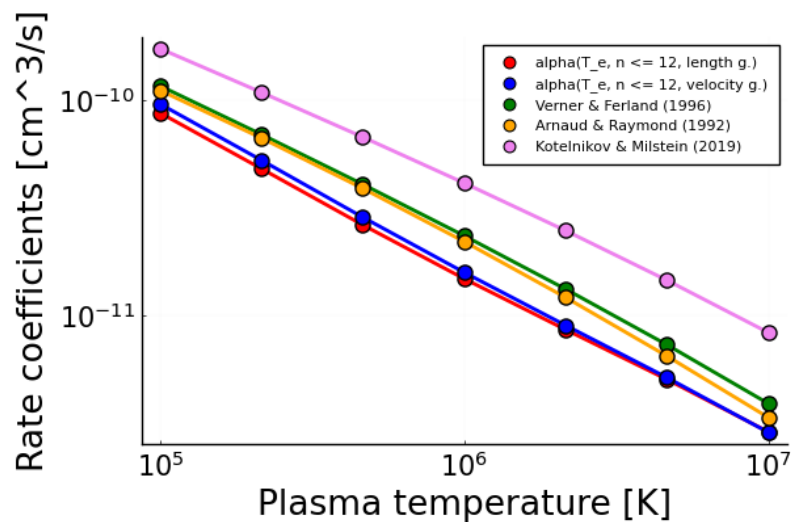
wb = Cascade.Simulation(Cascade.Simulation(), name=name, property=prop,
settings=simulationSettings, computationData=data )
perform(wb; output=true)
```

**Figure 3.** Input to the JAC toolbox for the cascade computation (upper panel) and simulation (lower panel) of RR plasma rate coefficients of initially helium-like  $\text{Fe}^{24+}$  ions. The total plasma rate coefficients are calculated for plasma temperatures  $10^5 \lesssim T_e \lesssim 10^7$  K, and by restricting the electron capture into  $n\ell$  shells with  $n = 2 \dots 12$  and  $\ell \leq f$ . While the cascade computations just generate all associated transition amplitudes, the subsequent simulation combines these data and extract the desired rate coefficients for a given set of temperatures. See the text for further discussion.

The cascade computation in the upper panel of Figure 3 is then followed by the `Cascade.Simulation` (lower panel) for extracting the desired RR plasma rate coefficients. Such cascade simulations generally combine the amplitudes and cross sections from above and (numerically) perform the integration over the relevant part of the electron continuum. A Gauss–Legendre integration has been implemented here, in contrast to a more natural Gauss–Laguerre integration scheme for plasma rate coefficients, in order to enable internally the use of the same many-electron amplitudes but for different temperatures of the plasma. These cascade simulations are typically much faster than the prior computations, and often quite similar simulations are performed repeatedly for different temperatures, initial levels, subshells of the captured electron, or other choices for the capture process, while still using the same transition data. For the computation of the total RR plasma rate coefficients, we just list the multipoles and the plasma temperatures in the input by specifying an instance of the data structure `Cascade.RrRateCoefficients(...)` as the requested property of our study. We also provide here the initial level number of the ground level as well as the temperatures of the plasma. Besides the choice of multipoles, the rate coefficients can also be restricted to selected fine-structure levels or subshells using a few optional arguments to `Cascade.RrRateCoefficients()`. Although, as mentioned before, such a separation into cascade computations and simulations includes fewer correlations in the representation of the fine-structure levels [54], it makes the estimation of plasma rate coefficients more flexible for atoms and ions with different shell structure. However, further work is likely

needed in order to accelerate and, perhaps, parallelize these computations for ions with complex shell structure of open  $d$ - and  $f$ -shell elements [55].

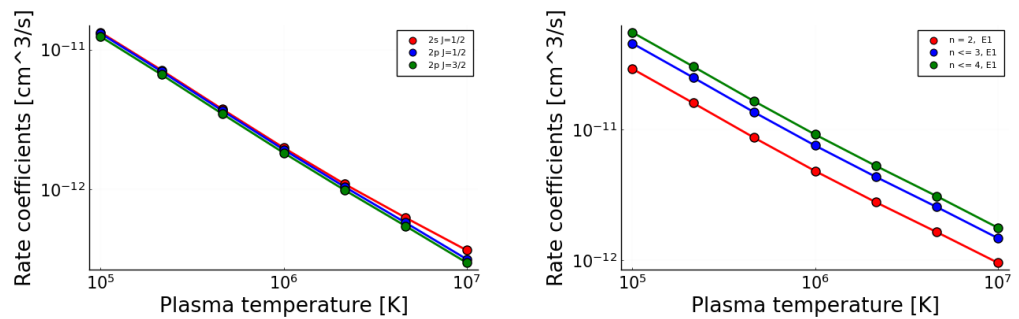
Figure 4 displays the total RR plasma rate coefficients as a function of the plasma temperature  $T_e$  for initially helium-like  $\text{Fe}^{24+}$  ions. Results from this work for an electron capture into  $n\ell$  shells with  $n = 2 \dots 12$  and  $\ell \leq f$  in length (red line) and velocity gauge (blue line) are compared with previous computations by Verner and Ferland ([13]; green line), the parametrization by Arnaud and Raymond ([10]; orange line) as well as the scaled analytical rates by Kotelnikov and Milstein ([42]; violet line). As expected, these total rate coefficients smoothly decrease as the temperature increases. In these computations, free electrons with 24 Gauss–Legendre distributed kinetic energies in the interval  $[0 \dots 5 \times k_B T_{e,\text{max}} \approx 4300 \text{ eV}]$  have been taken into account in order to facilitate a proper Maxwellian distribution of the free-electron continuum. The simulations then simply return the plasma rate coefficients for the given temperatures (and transition data). To ensure convergence of the results, a set of computations (and simulations) with different number of partial waves and shells typically needs to be performed and can be readily controlled by the cascade computations. For multiply charged ions, the total RR rates  $\alpha^{(\text{RR})}(T_e, i)$  converge rather rapidly for  $n \gtrsim 8$  and make the incorporation of high- $n$  shells rather unnecessary. Higher multipoles are negligible for most light and medium-heavy elements, such are iron, and are not shown separately in this figure. However, these contributions rapidly increase with  $Z$  owing to the different scaling of the multipole transitions [56,57]. Overall, these quite simple cascade simulations agree reasonably well with previous studies in the temperature region  $T_e = 10^5 - 5 \times 10^6 \text{ K}$ , while some larger discrepancies occur at high temperatures. We also note that some of these authors simply refer with their data to the final charge state of the ion. While this “final-ion” notation has its origin in the use of the Milne relation and the associated photoionization cross sections for ions in the final charge state, it makes the comparison of the radiative recombination process quite cumbersome, especially when discussed with regard to other processes.



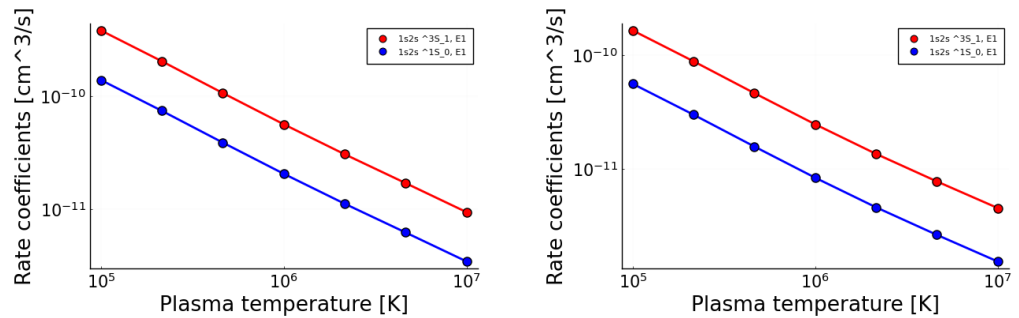
**Figure 4.** Total RR plasma rate coefficients as function of the (plasma) temperature  $T_e$  for initially helium-like  $\text{Fe}^{24+}$  ions. Results from this work with electron capture into the  $n\ell$  shells with  $n = 2 \dots 12$  and  $\ell \leq f$  in length (red line) and velocity gauge (blue line) are compared with previous computations by Verner and Ferland ([13]; green line), the parametrization by Arnaud and Raymond ([10]; orange line) and the scaled analytical rates by Kotelnikov and Milstein ([42]; violet line).

Figure 5 shows the fine-structure level- and shell-resolved RR plasma rate coefficients for the capture into various levels and shells. In the left panel of this figure, the fine-structure level-resolved rate coefficients are displayed for the  $2s J = 1/2$  (red line), the  $2p J = 1/2$  (blue line) and  $2p J = 3/2$  levels (green line), whereas the shell-resolved rate coefficients for the capture into  $n \leq 2$  (red line),  $n \leq 3$  (blue line), and  $n \leq 4$  (green

line) are seen on the right panel. Analog computations are performed again in Figure 6 but for the capture into the initially excited  $1s2s\ ^3S_1$  and  $1s2s\ ^1S_0$  levels. Data are shown for the total RR plasma rate coefficients  $\alpha^{(RR)}(T_e, i)$  for these two levels (left panel) as well as for just the capture into the  $1s^22s$  and  $1s2s^2$  configurations (right panel), respectively. A similar analysis of fine-structure level- or shell-resolved RR plasma rate coefficients can be performed with JAC for many other ions across the periodic table, though likely with some trade-off between the shell structure and the required computational effort and/or the accuracy of the individual rate coefficients. Such level- or shell-resolved plasma rate coefficients are needed in astrophysical simulations if, for instance, the electron temperature  $T_e$  and density  $n_e$  might change within the lifetime of meta-stable levels of the plasma ions and, hence, if the ions do not always recombine back to the ground level. Therefore, despite our treatment of the RR as a single-step cascade into different bound-state configurations, the simplicity and straightforward use of such a (cascade) model indeed facilitates studies on different ions and temperatures of interest.



**Figure 5.** The same as in Figure 4 but for the fine-structure and shell-resolved RR plasma rate coefficients. Left panel: Capture into the  $2s\ J = 1/2$  (red line), the  $2p\ J = 1/2$  (blue line) and  $2p\ J = 3/2$  level (green line). Right panel: Capture into all levels with  $n = 2$  (red line),  $n = 3$  (blue line), and  $n = 4$  (green line).



**Figure 6.** The same as in Figure 4 but for the capture into the initially excited  $i = 1s2s\ ^3S_1$  and  $1s2s\ ^1S_0$  levels. Data are shown for the total RR plasma rate coefficients  $\alpha^{(RR)}(T_e, i)$  for these two levels (left panel) as well as for just the capture into the  $1s^22s$  and  $1s2s^2$  configurations (right panel).

### 3.2. Trends for Multiply and Highly Charged Ions

Relativistic contributions to cross sections and plasma rate coefficients are known to become important for multiply and highly charged ions. For these ions, the (relativistic) motion of the electrons is well described by Dirac’s equation, which leads not only to a contraction of the charge density near the nucleus but also to the (well-known) fine-structure splitting as well as the coupling to different multipole fields beyond the (electric-) dipole field. At storage rings, for example, the radiative electron capture has been found to be dominant for the loss of ions from the beam, and this applies especially for collisions of high- $Z_p$  projectiles with low- $Z_t$  target atoms. For these targets, the capture cross sections of the circulating projectile ions with low or moderate energies are proportional to  $Z_p^5$

and, hence, their lifetimes fall by five orders of magnitude if the nuclear charge  $Z_p$  of the projectiles is increased by just a factor of ten [58].

To make the relativistic effects explicit, Figure 7 shows again the total RR plasma rate coefficients but for selected helium-like ions at temperatures  $10^5 \leq T_e \leq 10^7$  K. Rate coefficients are displayed for the capture into  $\text{Ne}^{8+}$  (red line),  $\text{Fe}^{24+}$  (blue line) and  $\text{W}^{72+}$  (green line). These rate coefficients rapidly increase with the nuclear charge owing to the increasing ionization potential, though the general trend as a function of the temperature remains the same. The right panel of this figure compares the ratio of the total plasma rate coefficients with regard to the E1 approximation for  $\text{W}^{72+}$  alone. Results are shown for E1 (red line), E1+M1 (blue line), E1+M1+E2 (green line), as well as the E1+M1+E2+M2 approximation (orange line), respectively. This comparison shows that the total rate coefficients at these temperatures are affected only very little by higher multipoles, and typically much less than the remaining uncertainties of the total values.

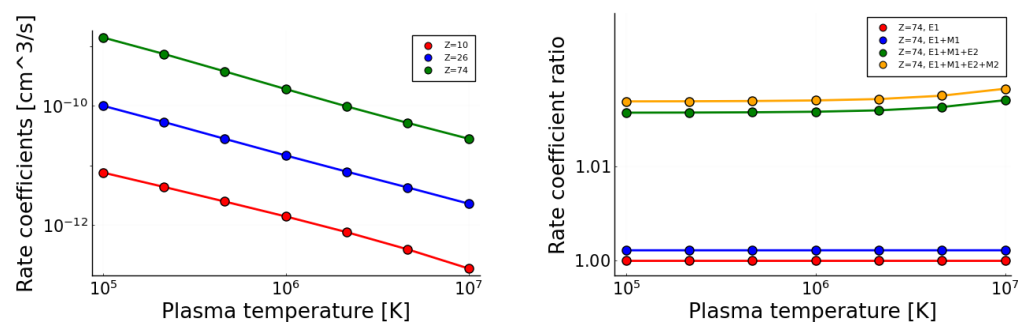


**Figure 7.** The same as in Fig. 4 but for the capture into selected helium-like ions. Left panel: RR plasma rate coefficients for  $\text{Ne}^{8+}$  (red line),  $\text{Fe}^{24+}$  (blue line),  $\text{W}^{72+}$  (green line), and by applying the electric-dipole (E1) approximation. Right panel: Comparison of the ratio of total plasma rate coefficients, normalized on the E1 approximation, for  $\text{W}^{72+}$  within the E1 (red line), E1+M1 (blue line), E1+M1+E2 (green line) and the E1+M1+E2+M2 approximation (orange line), respectively.

#### 4. Summary and Conclusions

RR plasma rate coefficients are relevant in astrophysics and fusion research for determining plasma temperatures, densities, or the distribution of charge states. Different fine-structure level- or shell-resolved as well as total plasma rate coefficients have to be considered in order to account for the ionization dynamics for given plasma conditions. We here demonstrate how RR plasma rate coefficients can be readily obtained by means of the JAC toolbox, and how easily computations can be performed for most ions across the periodic table. Apart from simple estimates of RR rate coefficients for rather a wide range of temperatures, emphasis has been placed on an improved control of the initial level population of ions in different charge states, the capture of electrons into individual shells, or the role of non-E1 contributions in the RR rate coefficients. In addition, the role of a relativistic Maxwell–Boltzmann distribution at high temperatures could easily be explored as well. In practice, fast and reliable access to the RR cross sections and plasma rate coefficients has been found to be central to studying the plasma dynamics beyond the equilibrium state as, for instance, seen in the time-evolution of kilonovae emissions [59].

While all examples above refer to the RR of initially helium-like ions, JAC’s radiative recombination (scheme) supports studies for many open-shell ions. This cascade scheme also helps overcome previous difficulties with the generation and application of a sufficiently large number of final states and/or electron continua in the treatment of the photorecombination process. Finally, the JAC toolbox also supports a good number of other processes, such as (line) energies, photoionization cross sections, and decay rates under different plasma environments [60].

**Author Contributions:** Conceptualization, S.F. and A.V.M.; software, S.F. and Z.W.; writing—review and editing, Z.W. All authors have read and agreed to the published version of the manuscript.

**Funding:** This research received no external funding.

**Data Availability Statement:** All data in Figures 4–7 can be reconstructed by means of the JAC toolbox, provided at the website [25].

**Conflicts of Interest:** The author declares no conflict of interest.

## References

1. Seaton, M.J. Radiative Recombination of Hydrogenic Ions. *Mon. Not. R. Astron. Soc.* **1959**, *119*, 81. [CrossRef]
2. Pequignot, D.; Petitjean, P.; Boisson, C. Total and effective radiative recombination coefficients. *Astron. Astrophys.* **1991**, *251*, 680.
3. Nahar, S.N. Electron-ion recombination rate coefficients and photoionization cross sections for astrophysically abundant elements. XI. N v–vi and F vii–viii for ultraviolet and x-ray modeling. *Astrophys. J. Suppl.* **2006**, *164*, 280. [CrossRef]
4. Surzhykov, A.; Fritzsche, S.; Stöhlker, T.; Tachenov, S. Polarization studies on the radiative recombination of highly charged bare ions. *Phys. Rev. A* **2003**, *68*, 022710. [CrossRef]
5. Mazzotta, P.; Mazzitelli, G.; Colafrancesco, S.; Vittorio, N. Ionization balance for optically thin plasmas: Rate coefficients for all atoms and ions of the elements H to Ni. *Astr. Astrophys. Suppl. Ser.* **1998**, *133*, 403. [CrossRef]
6. Trzhaskovskaya, M.B.; Nikulin, V.K. Radiative recombination and photoionization data for tungsten ions. Electron structure of ions in plasmas. *Atoms* **2015**, *3*, 86. [CrossRef]
7. Badnell, N.R. Radiative recombination data for modeling dynamic finite-density plasmas. *Astr. Astrophys. Suppl. Ser.* **2006**, *167*, 334. [CrossRef]
8. Raymond, J.C.; Cox, D.P.; Smith, B.W. Radiative cooling of a low-density plasma. *Astrophys. J.* **1976**, *204*, 290. [CrossRef]
9. Aldrovandi, S.M.V.; Pequignot, D. Radiative and dielectronic recombination coefficients for complex ions. *Astron. Astrophys.* **1973**, *25*, 137.
10. Arnaud, M.; Rothenflug, R. An updated evaluation of recombination and ionization rates. *Astron. Astrophys. Suppl. Ser.* **1985**, *60*, 425.
11. Landini, M.; Monsignori Fossi, B.C. Ion equilibrium for minor components in a thin plasma. *Astron. Astrophys.* **1991**, *91*, 183.
12. Arnaud, M.; Raymond, J. Iron ionization and recombination rates and ionization equilibrium. *Astrophys. J.* **1992**, *398*, 394. [CrossRef]
13. Verner, D.A.; Ferland, G.J. Atomic data for astrophysics. I. Radiative recombination rates for H-like, He-like, Li-like and Na-like ions over a broad range of temperature. *Astrophys. J. Suppl. Ser.* **1996**, *103*, 467. [CrossRef]
14. Summers, H.P. The ADAS User Manual, Version 2.6. Unpublished. 1996. Available online: <http://www.adas.ac.uk> (accessed on 18 February 2023).
15. Kim, Y.S.; Pratt, R.H. Direct radiative recombination of electrons with atomic ions: Cross sections and rate coefficients. *Phys. Rev. A* **1983**, *27*, 2913. [CrossRef]
16. Zhang, H.L.; Pradhan, A.K. Photoionization and recombination of Fe XIX. *Mon. Not. R. Astron. Soc.* **2000**, *313*, 13–20. [CrossRef]
17. Zatsarinny, O.; Gorcyca, T.; Fu, J.; Korista, K.T.; Badnell, N.R.; Savin, D.W. Dielectronic recombination data for dynamic finite-density plasmas. IX. The fluorine isoelectronic sequence. *Astron. Astrophys.* **2006**, *447*, 379. [CrossRef]
18. Ralchenko, Y. *Modern Methods in Collisional-Radiative Modeling of Plasma*; Springer: New York, NY, USA, 2016.
19. Ferland, G.J. The ionization balance of a non-equilibrium plasma. *Astron. Astrophys.* **2009**, *500*, 299. [CrossRef]
20. Rodriguez, R.; Espinosa, G.; Gil, J.M. Radiative properties for astrophysical plasma mixtures in nonlocal thermodynamic equilibrium. *Phys. Rev. E* **2018**, *98*, 033213. [CrossRef]
21. Fritzsche, S. A fresh computational approach to atomic structures, processes and cascades. *Comp. Phys. Commun.* **2019**, *240*, 1. [CrossRef]
22. Zatsarinny, O.; Gorczyca, T.W.; Korista, K.; Badnell, N.R.; Savin, D.W. Dielectronic recombination data for dynamic finite-density plasmas. VII. The neon isoelectronic sequence. *Astron. Astrophys.* **2004**, *426*, 699. [CrossRef]
23. Fritzsche, S. Dielectronic recombination strengths and plasma rate coefficients of multiply-charged ions. *Astron. Astrophys.* **2021**, *656*, A163. [CrossRef]
24. Fritzsche, S. The RATIP program for relativistic calculations of atomic transition, ionization and recombination properties. *Comp. Phys. Commun.* **2012**, *183*, 1525. [CrossRef]
25. Fritzsche, S. JAC: User Guide, Compendium & Theoretical Background. Unpublished. Available online: <https://github.com/OpenJAC/JAC.jl> (accessed on 10 December 2022).
26. Grant, I.P. *Relativistic Quantum Theory of Atoms and Molecules: Theory and Computation*; Springer: Berlin/Heidelberg, Germany, 2007.
27. Fritzsche, S. Large-scale accurate structure calculations for open-shell atoms and ions. *Phys. Scr.* **2002**, *T100*, 37. [CrossRef]
28. Eliav, E.; Fritzsche, S.; Kaldor, U. Electronic structure theory of the superheavy elements. *Nucl. Phys. A* **2015**, *944*, 518. [CrossRef]
29. Grant, I.P. Relativistic effects in atoms and molecules. In *Methods in Computational Chemistry*; Wilson, S., Ed.; Plenum: New York, NY, USA, 1988; Volume 2, p. 1.
30. Kabachnik, N.M.; Fritzsche, S.; Grum-Grzhimailo, A.N.; Meyer, M.; Ueda, K. Coherence and correlations in photoinduced Auger and fluorescence cascades in atoms. *Phys. Rep.* **2007**, *451*, 155. [CrossRef]
31. Fritzsche, S.; Fricke, B.; Sepp, W.D. Reduced  $L_1$  level-width and Coster-Kronig yields by relaxation and continuum interactions in atomic zinc. *Phys. Rev. A* **1992**, *45*, 1465. [CrossRef]

32. Nahar, S.N. Electron-ion recombination rate coefficients and photoionization cross sections for astrophysically abundant elements. VIII. Ar XIII with new features. *Astrophys. J. Suppl. Ser.* **2005**, *156*, 93. [[CrossRef](#)]
33. Trzhaskovskaya, M.B.; Nikulin, V.K.; Clark, R.E.H. Multipole and relativistic effects in radiative recombination process in hot plasmas. *Phys. Rev.* **2008**, *E78*, 035401(R). [[CrossRef](#)]
34. Fritzsche, S.; Palmeri, P.; Schippers, S. Atomic cascade computations. *Symmetry* **2021**, *13*, 520. [[CrossRef](#)]
35. Schippers, S.; Martins, M.; Beerwerth, R.; Bari, S.; Holste, K.; Schubert, K.; Viefhaus, J.; Savin, D.W.; Fritzsche, S.; Müller, A. Near L-edge single and multiple photoionization of singly charged iron ions. *Astrophys. J.* **2017**, *849*, 5. [[CrossRef](#)]
36. Beerwerth, R.; Buhr, T.; Perry-Sassmannshausen, A.; Stock, S.O.; Bari, S.; Holste, K.; Kilcoyne, A.L.D.; Reinwardt, S.; Ricz, S.; Savin, D.W.; et al. Near L-edge single and multiple photoionization of triply charged iron ions. *Astrophys. J.* **2019**, *887*, 189. [[CrossRef](#)]
37. Schippers, S.; Beerwerth, R.; Bari, S.; Buhr, T.; Holste, K.; Kilcoyne, A.L.D.; Perry-Sassmannshausen, A.; Phaneuf, R.A.; Reinwardt, S.; Savin, D.W.; et al. Near L-edge single and multiple photoionization of doubly charged iron ions. *Astrophys. J.* **2021**, *908*, 52. [[CrossRef](#)]
38. Schippers, S.; Beerwerth, R.; Abrok, L.; Bari, S.; Buhr, T.; Martins, M.; Ricz, S.; Viefhaus, J.; Fritzsche, S.; Müller, A.; et al. Prominent role of multielectron processes in K-shell double and triple photodetachment of oxygen anions. *Phys. Rev. A* **2016**, *94*, 041401(R). [[CrossRef](#)]
39. Fritzsche, S. Photon emission from hollow ions near surfaces. *Atoms* **2022**, *10*, 37. [[CrossRef](#)]
40. Hitomi Collaboration; Aharonian, F.; Akamatsu, H.; Akimoto, F.; Allen, S.W.; Angelini, L.; Audard, M.; Awaki, H.; Axelsson, M.; Bamba, A.; et al. Atomic data and spectral modeling constraints from high-resolution X-ray observations of the Perseus cluster with Hitomi. *Public. Astron. Soc. Japan* **2018**, *70*, 12. [[CrossRef](#)]
41. Kramers, H. On the theory of X-ray absorption and of continuous X-ray spectrum. *Phil. Mag.* **1923**, *46*, 836. [[CrossRef](#)]
42. Kotelnikov, I.A.; Milstein, A.I. Electron radiative recombination with a hydrogen-like ion. *Phys. Scr.* **2019**, *94*, 055403. [[CrossRef](#)]
43. Perry-Sassmannshausen, A.; Buhr, T.; Borovik, A., Jr.; Martins, M.; Reinwardt, S.; Ricz, S.; Stock, S.; Trinter, F.; Müller, A.; Fritzsche, S.; et al. Multiple photodetachment of carbon anions via single and double core-hole creation. *Phys. Rev. Lett.* **2020**, *124*, 083203. [[CrossRef](#)] [[PubMed](#)]
44. Schippers, S.; Hamann, A.; Perry-Sassmannshausen, A.; Buhr, T.; Müller, A.; Martins, M.; Reinwardt, S.; Trinter, F.; Fritzsche, S. Multiple photodetachment of oxygen anions via K-shell excitation and ionization: Direct double-detachment processes and subsequent deexcitation cascades *Phys. Rev. A* **2022**, *106*, 013114. [[CrossRef](#)]
45. Fritzsche, S.; Surzhykov, A. Approximate atomic Green functions. *Molecules* **2021**, *26*, 2660. [[CrossRef](#)]
46. Julia 1.8 Documentation. Available online: <https://docs.julialang.org/> (accessed on 10 December 2021).
47. Bezanson, J.; Chen, J.; Chung, B.; Karpinski, S.; Shah, V.B.; Vitek, J.; Zoubritzky, L. Julia: Dynamism and performance reconciled by design. *Proc. Acm Program. Lang.* **2018**, *2*, 120. [[CrossRef](#)]
48. McLaughlin, D.J.; Hahn, Y. Scaling behavior of radiative recombination cross sections and rate coefficients. *Phys. Rev. A* **1991**, *43*, 1313. [[CrossRef](#)] [[PubMed](#)]
49. Saha, B.; Fritzsche, S. Influence of dense plasma on the low-lying transitions in Be-like ions: Relativistic multiconfiguration Dirac-Fock calculations. *J. Phys. B* **2007**, *40*, 259. [[CrossRef](#)]
50. Mao, J.; Kaastra, J. Parameterization of the level-resolved radiative recombination rate coefficients for the SPEX code. *Astron. Astrophys.* **2016**, *587*, A84. [[CrossRef](#)]
51. Ralchenko, Y. Collisional-Radiative Modeling for Highly-Charged Ions of Tungsten. *Plasma Fusion Res.* **2013**, *8*, 2503024. [[CrossRef](#)]
52. Barfield, W.D. Partial photoionization cross sections and radiative recombination rate coefficients for lithium-like ions. *Astrophys. J.* **1979**, *29*, 856. [[CrossRef](#)]
53. Pradhan, A.K. Radiative recombination of the ground state of lithium-like ions. *Astrophys. J.* **1983**, *270*, 339. [[CrossRef](#)]
54. Fritzsche, S.; Surzhykov, A.; Stöhlker, T. Radiative recombination into high-Z few-electron ions: Cross sections and angular distributions. *Phys. Rev. A* **2005**, *72*, 012704. [[CrossRef](#)]
55. Fritzsche, S. Level structure and properties of open *f*-shell elements. *Atoms* **2022**, *10*, 7. [[CrossRef](#)]
56. Rose, M.E. *Multipole Fields*; John Wiley & Sons: New York, NY, USA, 1955.
57. Jitrik, O.; Bunge, C.F. Transition probabilities for hydrogen-like atoms. *J. Phys. Chem. Ref. Data* **2004**, *33*, 1059. [[CrossRef](#)]
58. Eichler, J.; Meyerhof, W.E. *Relativistic Atomic Collisions*; Academic Press: Cambridge, MA, USA, 1995.
59. Piron, R.; Gilleron, F.; Aglitskiy, Y.; Chung, H.-K.; Fontes, C.J.; Hansen, S.B.; Marchuk, O.; Scott, H.A.; Stambulchik, E.; Ralchenko, Y. Review of the 9th NLTE code comparison workshop. *High Energy Density Phys.* **2017**, *23*, 38. [[CrossRef](#)] [[PubMed](#)]
60. Deprince, J.; Bautista, M.A.; Fritzsche, S.; García, J.A.; Kallman, T.R.; Mendoza, C.; Palmeri, P.; Quinet, P. Plasma environment effects on K lines of astrophysical interest. I. Atomic structure, radiative rates, and Auger widths of oxygen ions. *Astron. Astrophys.* **2019**, *624*, A74. [[CrossRef](#)]

**Disclaimer/Publisher's Note:** The statements, opinions and data contained in all publications are solely those of the individual author(s) and contributor(s) and not of MDPI and/or the editor(s). MDPI and/or the editor(s) disclaim responsibility for any injury to people or property resulting from any ideas, methods, instructions or products referred to in the content.